Structural Evolution of Copper-Oxo Sites in Zeolites upon the Reaction with Methane Investigated by Means of Cu K-edge X-ray Absorption Spectroscopy

Artsiusheuski, Mikalai A.; Safonova, Olga; Palagin, Dennis; van Bokhoven, Jeroen A.; Sushkevich, Vitaly L.

Important note
To cite this publication, please use the final published version (if applicable).
Please check the document version above.

Structural Evolution of Copper-Oxo Sites in Zeolites upon the Reaction with Methane Investigated by Means of Cu K-edge X-ray Absorption Spectroscopy

Mikalai A. Artsiusheuski, Olga Safonova, Dennis Palagin, Jeroen A. van Bokhoven,* and Vitaly L. Sushkevich*

Read Online

ACCESS | Metrics & More | Article Recommendations | Supporting Information

ABSTRACT: The structure of copper sites formed under an oxidative environment and their evolution in the course of the reaction with methane at elevated temperature was investigated by means of Cu K-edge X-ray absorption spectroscopy for a series of copper-containing MFI, MOR, and FAU zeolites. The pretreatment in oxygen at 723 K leads to the formation of copper(II)-oxo sites, whose nature depends on the framework type. Dimeric species are formed in CuMFI material, dimeric and monomeric sites coexist in CuMOR, and agglomerated copper-oxo nanoclusters are found in large-pore copper-containing faujasite (CuFAU). For all studied materials, the reaction with methane resulted in the exclusive formation of copper(I) species; no formation of metallic copper was detected even at 748 K. The nature of formed copper(I) species is governed by the structure of corresponding copper(II) centers. In particular, monomeric and dimeric copper(II)-oxo sites hosted in CuMOR and CuMFI are transformed into isolated copper(I) cations coordinated to ion-exchange positions of the zeolite. Contrarily, copper(II)-oxo clusters present in CuFAU undergo restructuring with only a partial loss of extra-framework oxygen and form aggregated species with a structure similar to that of bulk copper(I) oxide.
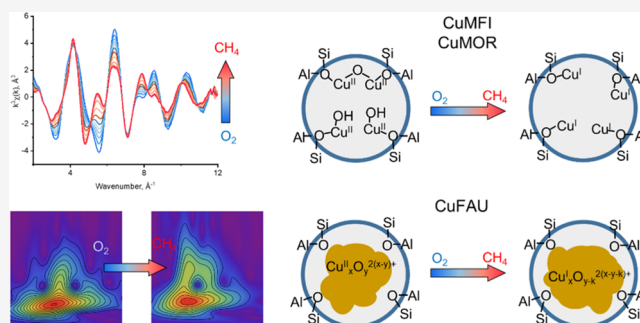
1. INTRODUCTION

Copper-containing zeolites are known as industrial catalysts for the DeNOx process[1−6] and active materials for direct methane oxidation to methanol (DMTM).[7−11] In both mentioned processes, the transformation between Cu^I and Cu^{II} oxidation states takes place, resulting in interconversion between corresponding copper(I) and copper(II) sites. Understanding the evolution of the structure of copper sites under reactive conditions is essential for the fundamental understanding of the mentioned processes, aiding the design of better-performing materials.

The pretreatment of copper-containing zeolites in oxidative conditions is the first step in both selective catalytic reduction (SCR) of nitrogen oxides and DMTM processes.[4,12] The structure of copper(II) sites in zeolites formed under oxidative pretreatment has been studied for several decades. The zeolite framework type,[10,13−18] Si/Al ratio,[10,14,19−21] copper loading,[3,22,23] and the nature of co-cations[24,25] influence the copper(II) speciation. Monomeric,[19,23,26] dimeric mono-μ-oxo,[8,18,27,28] bis-μ-oxo,[7,29] μ-1,2-peroxo,[14,25,30] trimeric,[31,32] and oligomeric[17,33] motifs were proposed for copper(II) sites hosted in zeolites. Moreover, some recent studies suggest that not one particular type, but a mixture of different copper(II) sites may coexist in the copper-containing zeolite.[23,28,34] All this

points to the existence of a variety of copper(II) sites, which likely behave differently under reactive conditions.

When the activated material containing copper(II) sites is exposed to the environment containing a reducing agent, as happens during SCR and DMTM, a change of the oxidation state and local environment of copper atoms takes place. The nature of the reducing agent and the reaction temperature affect the state of copper. For instance, the reduction in hydrogen below 473 K leads to the formation of copper(I) sites in copper-containing FAU and MFI materials.[35,36] Above 573 K, the reduction proceeds further, resulting in the formation of metallic copper, which migrates out of the zeolite crystals and forms metallic particles.[35,37−41] Notably, only part of metallic copper can be reoxidized to copper(II) extra-framework cations, while the rest of copper forms copper(II) oxide particles. In contrast to hydrogen, employing carbon monoxide as a reducing agent for
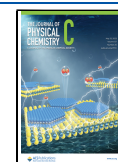
Figure 1. Schematic representation of the experimental protocol employed for the acquisition of XAS spectra corresponding to different stages of the reaction between activated materials and methane.

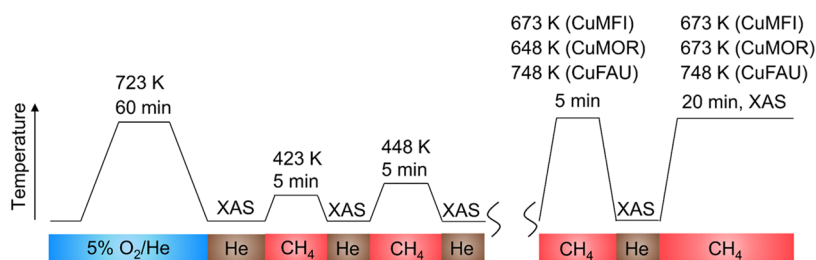copper(II)-containing FAU and MFI zeolites leads to the formation of exclusively Cu^I sites even at a temperature as high as 773 K.[42−44] Notably, the corresponding copper(I) species end up in a form of a $Cu^I(CO)^+$ complex of a carbon monoxide ligand strongly coordinated to a copper(I) cation.[42,43] At a high CO pressure and ambient temperature, monocarbonyl species can be reversibly transformed into $Cu^I(CO)_2^+$ dicarbonyl species.[45] In the presence of ammonia, copper(II) species in CHA and MOR zeolites are reduced into $Cu^I(NH_3)_x^+$ ($x = 2−4$) cations between 473 and 773 K. Notably, these cations possess high mobility, hence enabling migration of copper between different ion-exchange positions and justifying high catalytic activity in the SCR process.[46−49]

The possibility of copper-containing zeolitic materials to selectively oxidize methane has been demonstrated,[7] hence bringing attention to the reaction between copper(II) sites and methane. The evolution of different copper(II) sites in the course of the reaction with methane was mainly studied for dimeric sites hosted in copper-containing MOR materials. Borfecchia et al. studied the reaction of copper-containing CHA and MOR with methane at 473 K and found that partial copper(II) reduction does not lead to significant rearrangement in the structure of copper sites for either material.[47] In our recent work, we came to a similar conclusion, showing the stability of the Cu−Cu motif during the partial reduction of copper(II) mono-μ-oxo dimeric sites in CuMOR with methane at 483 K.[23] Alternatively, Deplano et al.[50] recently demonstrated that the reaction of oxygen-activated copper-containing mordenite with methane at 523 K leads to at least partial reduction of dimeric copper(II) sites into isolated copper(I) species. Lomachenko et al. examined the effect of reaction conditions on the copper speciation for copper-containing mordenite and found that the longer reduction time promotes the rearrangement of dicopper core into isolated copper(I) species.[20] This indicates that the conditions of the reaction between copper(II) sites and methane influence the resulting structure of copper(I) species. However, the fate of copper(II) sites upon the complete reduction of methane is not clarified yet. Even more importantly, the evolution of various active sites, i.e., dimeric sites hosted in zeolites of topologies other than MOR, and monomeric and oligomeric copper(II) centers, upon a reaction with methane, is poorly studied so far.

Establishing the structure of copper sites in zeolites and tracking their evolution during the redox reactions appear to be challenging due to the low content of active species and intrinsic capability to form mixtures of sites possessing different structure. X-ray absorption spectroscopy (XAS) is a powerful element-specific technique to monitor the oxidation state and the local environment of copper atoms in the course of the reaction with methane. Commonly, two subtechniques are distinguished in XAS: the X-ray absorption near-edge structure (XANES) and

extended X-ray absorption fine structure (EXAFS).[51−54] Applied to copper-containing zeolites, the first technique allows monitoring the oxidation state and the changes in the local symmetry of copper sites.[17,47,55] The use of reference systems allows one to determine the fraction of different copper sites by analyzing XANES using linear combination fitting.[15,16,56,57] *Ab initio* modeling of XANES spectra is possible; however, derivation of structural information solely based on XANES data remains challenging.[58,59] The spectral shape of EXAFS is determined by the local environment of the absorbing atom, yielding distances, coordination numbers, types of neighbors, and the Debye−Waller factor of the scattering neighbors.[53,60] Modeling and fitting of EXAFS are well-developed and widely utilized procedures, and there are several validated algorithms and software packages applied for this purpose.[61−63] Notably, the simultaneous analysis of both XANES and EXAFS data enables obtaining complementary information on the oxidation state, the symmetry, and the geometrical environment of the absorbing atom.

In the present work, we employed Cu K-edge X-ray absorption spectroscopy to investigate the structure of the copper sites hosted in zeolites of various topologies and monitored the evolution of these sites upon a reaction with methane at different temperatures. The nature of copper(II) sites and of zeolite frameworks determines the structure of copper(I) species formed in the course of the reaction with methane. MFI, MOR, and FAU frameworks stabilize dimeric, coexisting dimeric and monomeric, and oligomeric copper(II)-oxo sites, respectively, after oxygen pretreatment. The reaction with methane leads to the formation of isolated copper(I) monomers in the case of CuMFI and CuMOR, while rearrangement into copper(I)-oxo clusters takes place for CuFAU.

2. EXPERIMENTAL SECTION

2.1. Materials Preparation. The commercial zeolites MOR (CBV 10 ADS, Si/Al = 6.5, in sodium form), MFI (CBV2314, Si/Al = 12, in ammonium form), and FAU (CBV300, Si/Al = 2.5, in ammonium form) were purchased from Zeolyst and used as the starting materials.

The parent mordenite was converted to the ammonium form using the experimental protocols described elsewhere.[15,16] In order to obtain copper form of zeolites, the ion exchange was performed as follows: 10 g of the ammonium form of zeolite was added to 500 mL of a 0.05 M aqueous solution of copper(II) nitrate (99%, Sigma-Aldrich), and the suspension was stirred for 12 h at 323 K followed by filtration through the paper filter. Afterward, the material was washed with deionized water and dried at 393 K for 12 h. The ion-exchange procedure was repeated three times in order to obtain complete ion exchange.

The resulting materials were ascribed as CuZEO, where ZEO represents framework type of parent zeolite. Elemental composition of resulting materials is presented in Table S1.

2.2. Cu K-Edge X-ray Absorption Spectroscopy (XAS) Measurements. The measurements of Cu K-edge X-ray absorption spectra (XAS) were carried out at the SuperXAS beamline, Swiss Light Source, Switzerland. For the collimation of a polychromatic beam, a silicon-coated mirror at 2.5 mrad was applied. Afterward, the beam was monochromatized using a Si(111) channel-cut monochromator. The monochromatized beam was focused to a linear size of 1500 $\mu m \times 300$ μm. The spectra acquisition was performed in a transmission mode using the nitrogen-filled ionization chamber detectors. The energy was calibrated using the reference copper foil spectra, which were acquired simultaneously to each measurement.

The experimental protocol for acquisition of XAS measurements at different stages of the reaction between activated material and methane is presented in Figure 1.

For measurements, around 5 mg of each sample was placed between quartz wool plugs in the quartz capillary with the outer diameter equal to 1.5 mm and a wall thickness of 0.01 mm. The capillary was mounted in the custom-made cell[64] equipped with a heating system and a thermocouple was placed in the sample layer, enabling precise control of the temperature. The sample was heated up to 723 K with a rate of 8 K·min^{-1} in a flow of 5% O_2/Ar and kept at this temperature for 1 h for the activation. Afterward, the sample was cooled with a rate of 30 K·min^{-1} to ambient temperature, purged with helium for 10 min, followed by an acquisition of 1200 repetitive XAS spectra during 20 min. At the next stage, a methane flow was introduced and the sample was heated with a rate of 30 K·min^{-1} up to the desired temperature, kept for 5 min, and cooled to the ambient temperature followed by a gas switch to helium and the XAS spectra acquisition. The temperature of the reaction with methane was gradually increased starting from 423 K with a 25 K increment to 673 K for CuMOR and CuMFI and 748 K for CuFAU. Additionally, XAS spectra at the highest reaction temperature were acquired for each sample. All gas sources (grade 6.0) were equipped with moisture traps to exclude the presence of water vapors; the flows were set at 10 mL·min^{-1} and monitored by digital mass flow controllers (Bronkhorst).

2.3. Cu K-Edge X-ray Absorption Spectra Processing. The acquired XAS spectra were averaged to increase the signal-to-noise ratio using ProXAS software.[65] Athena software from the Demeter package was used for the normalization and background subtraction.[61] For the analysis of EXAFS, the Artemis software package was used. The phase and amplitude were calculated using the FEFF6 code.[66] For the Fourier transform (FT), k^3-weighting was used in the k-range of 3.0−16.0 Å^{-1}.

For the wavelet transform, k^3-weighted EXAFS spectra were used. Wavelet transformation was performed using the Morlet wavelet mother function within the k-range of 1−15 Å^{-1}. Mathematica software[67] was used for the continuous wavelet transformation with subsequent visualization as a two-dimensional (2D) contour plot projection of a three-dimensional (3D) graph.

2.4. Linear Combination Fitting (LCF) Analysis of XANES Spectra. For linear combination fitting (LCF) of XANES spectra, the spectra corresponding to oxygen-activated materials were used as standards of copper(II), and the spectra after a reaction with methane at the highest temperature and acquired at this temperature were used as copper(I) standard.

2.5. EXAFS Fitting: The CuMFI and CuMOR Cases. For spectra corresponding to CuMFI and CuMOR materials, the fitting was performed in k^3-weighted R-space in the 1.0−3.0 Å region, except for the spectra acquired at high temperature, where region 1.0−2.2 Å was employed for the fitting. The amplitude reduction factor extracted from the fitting of Cu foil equals to 0.90 and was used throughout the study.

A periodic structure of dicopper mono-μ-oxo species located in the MOR framework and optimized with density functional theory (DFT) was used as the initial model for the EXAFS spectra corresponding to CuMOR and CuMFI materials.[17] The optimized geometry was used as the initial model, based on which scattering paths were calculated using the FEFF code. A singe Cu−O scattering path was used for the 1st coordination sphere, and the presence of Cu−Al(Si) and Cu−Cu single scattering paths simultaneously was taken into account to describe the 2nd coordination sphere[10,17,47,68] (Figure S5). The coordination number, the distance to the scattering atom, and the Debye−Waller factor were used as the fitted parameters for each scattering path. Together with the adjustment to the absorption energy, it resulted in 10 variables for each spectrum corresponding to CuMOR and CuMFI materials. The employing the k-range of 3.0−16.0 Å^{-1} for the FT provides more than 15 independent points according to the Nyquist theorem,[69] enabling the possibility of high-quality fitting.

2.6. EXAFS Fitting: The CuFAU Case. In the case of CuFAU, the DFT-optimized structure of copper-oxo cluster having all copper atoms in the Cu^{II} oxidation state and located in the FAU structure has been used as a starting guess to fit the spectrum of oxygen-activated material (corresponding material is denoted as "Cu^{II}FAU").[17] A singe Cu−O scattering path was used for the 1st coordination sphere, and the second sphere can be described as a superposition of one Cu−Al(Si) and two distinct Cu−Cu single scattering paths (Figure S5). To fit the EXAFS spectra of CuFAU after the reaction with methane at 748 K (denoted as "Cu^{I}FAU"), the following paths were employed: single Cu−O in the 1st coordination sphere and superposition of Cu−Al(Si) and Cu−Cu and Cu−O paths in the 2nd coordination sphere (Figure S5). All intermediate EXAFS spectra of CuFAU reacted with methane at temperature lower than 748 K were fitted as linear combination (LCF) of the Cu^{I}FAU and Cu^{II}FAU spectra, representing an intermediate stage of transformation between two states described above.

To visualize the changes occurring in the course of the CuFAU reduction with methane, the cumulative copper coordination number and the average distance to copper and aluminum (and/or silicon) atoms at different stages of the reaction were calculated. The averaged oxygen, aluminum (and/or silicon), and cumulative copper coordination numbers were calculated as follows

$$N(\text{O}) = f(\text{Cu}^{II}\text{FAU}) \cdot N_{\text{Cu}^{II}\text{FAU}}(\text{O})$$
$$+ f(\text{Cu}^{I}\text{FAU}) \cdot N_{\text{Cu}^{I}\text{FAU}}(\text{O})$$

$$N(\text{Al(Si)}) = f(\text{Cu}^{II}\text{FAU}) \cdot N_{\text{Cu}^{II}\text{FAU}}(\text{Al(Si)})$$
$$+ f(\text{Cu}^{I}\text{FAU}) \cdot N_{\text{Cu}^{I}\text{FAU}}(\text{Al(Si)})$$

$$N(\text{Cu}) = f(\text{Cu}^{II}\text{FAU}) \cdot \sum N_{\text{Cu}^{II}\text{FAU}}(\text{Cu})$$
$$+ f(\text{Cu}^{I}\text{FAU}) \cdot N_{\text{Cu}^{I}\text{FAU}}(\text{Cu})$$
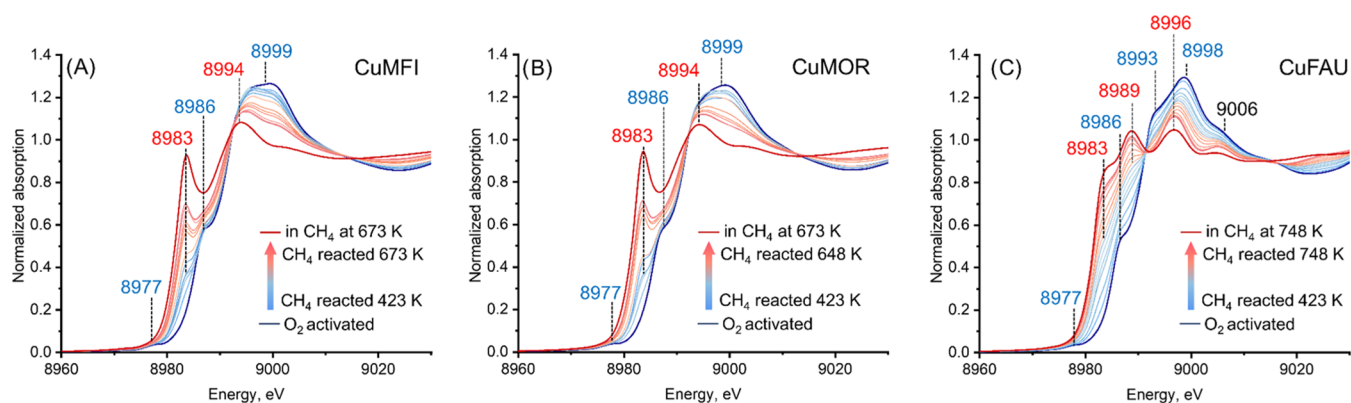
Figure 2. XANES spectra acquired at different stages of the reaction between CuMFI (A), CuMOR (B), and CuFAU (C) and methane. Labels of the signals corresponding to Cu^{II} and Cu^{I} species are colored in blue and red, respectively. The spectra shown in blue thick lines correspond to oxygen-activated materials and are acquired at ambient temperature, the spectra shown in thin lines are related to the state of the materials after the reaction with methane at various temperature and are acquired at ambient temperature, and the spectra shown in red thick lines correspond to the highest reaction temperature with acquisition exactly at the corresponding temperature without cooling.

where $f(Cu^{II}FAU)$ and $f(Cu^{I}FAU)$ are the fractions of Cu^{II}FAU and Cu^{I}FAU spectra determined from LCF of EXAFS data, respectively; $N_{Cu^{II}FAU}(O)$ and $N_{Cu^{I}FAU}(O)$ are the coordination numbers due to oxygen scattering atoms in the first coordination sphere; $N_{Cu^{II}FAU}(Al(Si))$ and $N_{Cu^{I}FAU}(Al(Si))$ are the coordination numbers corresponding to aluminum (and/or silicon) scatterers; and $\sum N_{Cu^{II}FAU}(Cu)$ and $N_{Cu^{I}FAU}(Cu)$ is the sum of coordination numbers due to all copper scatterers determined from fit of Cu^{II}FAU and Cu^{I}FAU spectra, respectively. The summation was done to take into account the presence of two distinct copper scattering atoms in the model used for the fitting of the Cu^{II}FAU spectrum.

The averaged distance to copper or aluminum (and/or silicon) scatterers was calculated as follows

$$R(Al(Si)) = [f(Cu^{II}FAU) \cdot N_{Cu^{II}FAU}(Al(Si)) \cdot R_{Cu^{II}FAU}(Al(Si))$$
$$+ f(Cu^{I}FAU) \cdot N_{Cu^{I}FAU}(Al(Si)) \cdot R_{Cu^{I}FAU}(Al(Si))] /$$
$$[f(Cu^{II}FAU) \cdot N_{Cu^{II}FAU}(Al(Si)) + f(Cu^{I}FAU) \cdot N_{Cu^{I}FAU}(Al(Si))]$$

$$R(Cu) = \left\{ f(Cu^{II}FAU) \cdot \sum_i [N^i_{Cu^{II}FAU}(Cu) \cdot R^i_{Cu^{II}FAU}(Cu)] \right.$$
$$\left. + f(Cu^{I}FAU) \cdot N_{Cu^{I}FAU}(Cu) \cdot R_{Cu^{I}FAU}(Cu) \right\} \Big/$$
$$\left\{ f(Cu^{II}FAU) \cdot \sum_i N^i_{Cu^{II}FAU}(Cu) + f(Cu^{I}FAU) \cdot N_{Cu^{I}FAU}(Cu) \right\}$$

where $R_{Cu^{I}FAU}(Al(Si))$ and $R_{Cu^{II}FAU}(Al(Si))$ are the distances to aluminum (and/or silicon) and copper scatterers, respectively, and $R_{Cu^{I}FAU}(Cu)$ and $R^i_{Cu^{II}FAU}(Cu)$ are distances to copper scatterers calculated from the fit of Cu^{I}FAU and Cu^{II}FAU spectra, respectively. The summation accounts for the presence of two pathways involving copper–copper scattering in the model applied for the fitting of Cu^{II}FAU spectra.

The reported errors of fitted parameters correspond to the standard deviation. The errors in the calculated parameters, namely averaged coordination numbers and averaged distances, were estimated as an error of an indirect measurement with coordination numbers and interatomic distances obtained from fitting of Cu^{I}FAU and Cu^{II}FAU spectra considered as independent parameters.

3. RESULTS

3.1. Cu K-Edge XANES Spectra upon the Reaction with Oxygen and Methane. Figure 2 shows the XANES spectra acquired at different stages of the reaction between oxygen-activated materials and methane. All spectra corresponding to the oxygen-activated state of the materials (dark blue thick lines) in the 8970−9000 eV energy region contain the features typical of copper(II) species: a weak peak at 8977 eV due to the 1s → 3d quadrupole transition, the shoulder at 8986 eV, and the peak at 8999 eV corresponding to the dipole 1s → 4p transitions.[70−74] In contrast, the 8990−9020 eV region of the spectra of oxygen-activated materials looks significantly different (Figures 2 and S3). In the spectra corresponding to CuMFI and CuMOR, there is one broad asymmetric peak at 8999 eV, while the spectrum of oxygen-activated CuFAU comprises a sharp resolved signal at 8998 eV with shoulders at about 8993 and 9006 eV.

The reaction between activated samples and methane leads to the appearance of a pre-edge peak centered at 8983 eV, which is characteristic of copper(I) species.[70−74] Notably, in the spectra of CuFAU, an additional pre-edge feature at 8989 eV appears during the reaction with methane starting at 548 K.[16,17] A gradual increase in the reaction temperature results in a progressive decline of the signals due to copper(II) and development of signals corresponding to copper(I) species. For each sample, the spectra corresponding to the reaction with methane at the highest temperature (dark red thick lines in Figure 2) contain no peak at 8977 eV, indicating the complete conversion of copper(II). The reaction with methane leads to the decrease in the intensity of the white line, pointing to a decrease of the coordination number in the first coordination sphere in the course of reduction[20,47] (*vide infra*). Apart from that, the position of the white line shifts: the final spectra of CuMOR and CuMFI have their maximum at about 8994 eV, and in the corresponding spectra of CuFAU, it is located at about 8996 eV. A notable isosbestic points are evident in Figure 2A−C at 8991 eV, suggesting the gradual transformation between two states of copper atoms in oxygen-activated and methane-reacted materials. For all materials, linear combination fitting of the XANES spectra shows that upon an increase in the temperature of the reaction with methane, the gradual reduction of copper(II) to copper(I) takes place (Figure S4).

3.2. Cu K-Edge EXAFS Spectra in the Course of the Reaction with Methane. Figures 3 and 4 show the k^3-

Figure 3. k^3-weighted $\chi(k)$ spectra (A) and the corresponding phase-uncorrected magnitude (B) and real part (C) of Fourier transform and contour plots of the wavelet transform (D) acquired at different stages of the reaction between CuMFI with methane. The spectra shown in blue thick lines correspond to oxygen-activated CuMFI and are acquired at ambient temperature, the spectra shown in thin lines are related to the state of the material after the reaction with methane at various temperatures and are acquired at ambient temperature, and the spectra shown in red thick lines correspond to the highest reaction temperature with acquisition at 673 K without cooling.

Figure 4. k^3-weighted $\chi(k)$ spectra (A) and the corresponding phase-uncorrected magnitude (B) and real part (C) of Fourier transform and contour plots of wavelet transform (D) acquired at different stages of the reaction between CuMOR material with methane. The spectra shown in blue thick lines correspond to oxygen-activated CuMOR and are acquired at ambient temperature, the spectra shown in thin lines are related to the state of the material after the reaction with methane at various temperatures and are acquired at ambient temperature, and the spectra shown in red thick lines correspond to the highest reaction temperature with acquisition at 673 K without cooling.

weighted $\chi(k)$ spectra and the corresponding phase-uncorrected Fourier transform (FT) and wavelet transform (WT) of Cu K-edge EXAFS spectra of CuMFI and CuMOR, respectively, after

reaction at different temperatures. The evolution of the spectra in the course of copper reduction with methane occurs in a very similar manner for both materials: the gradual increase in
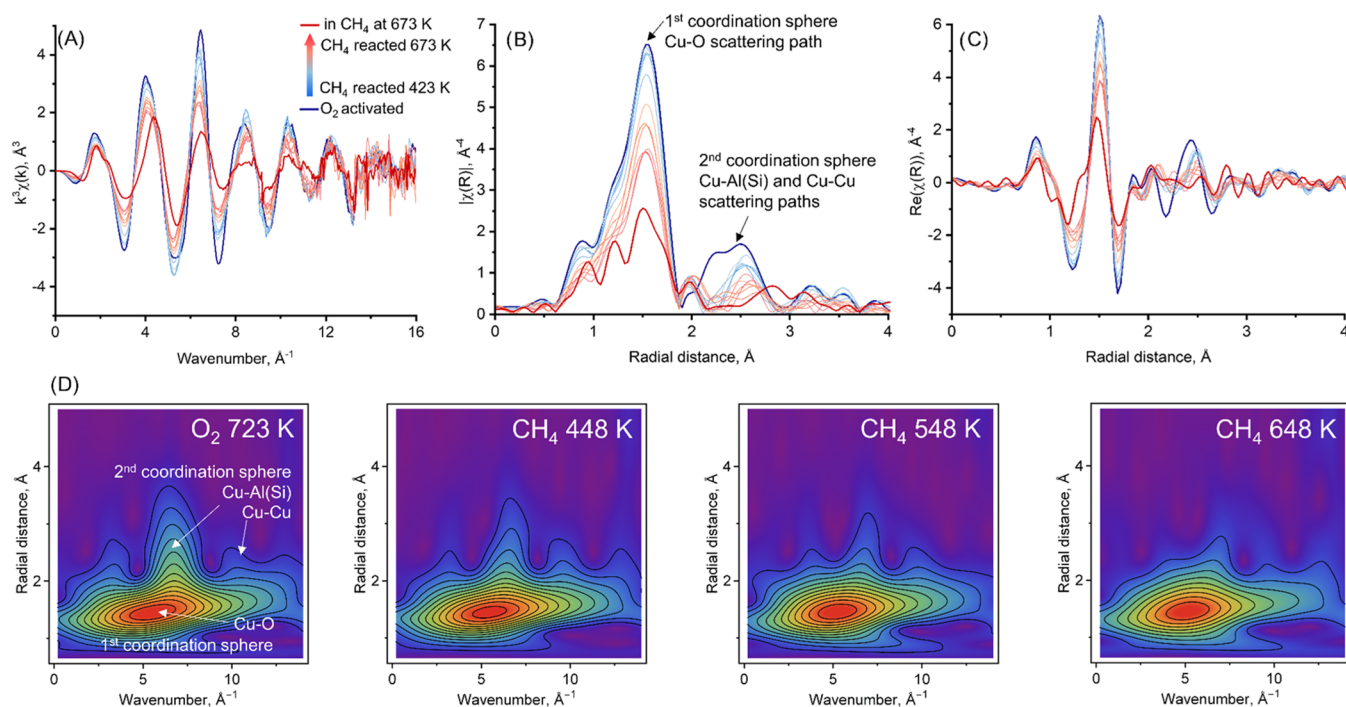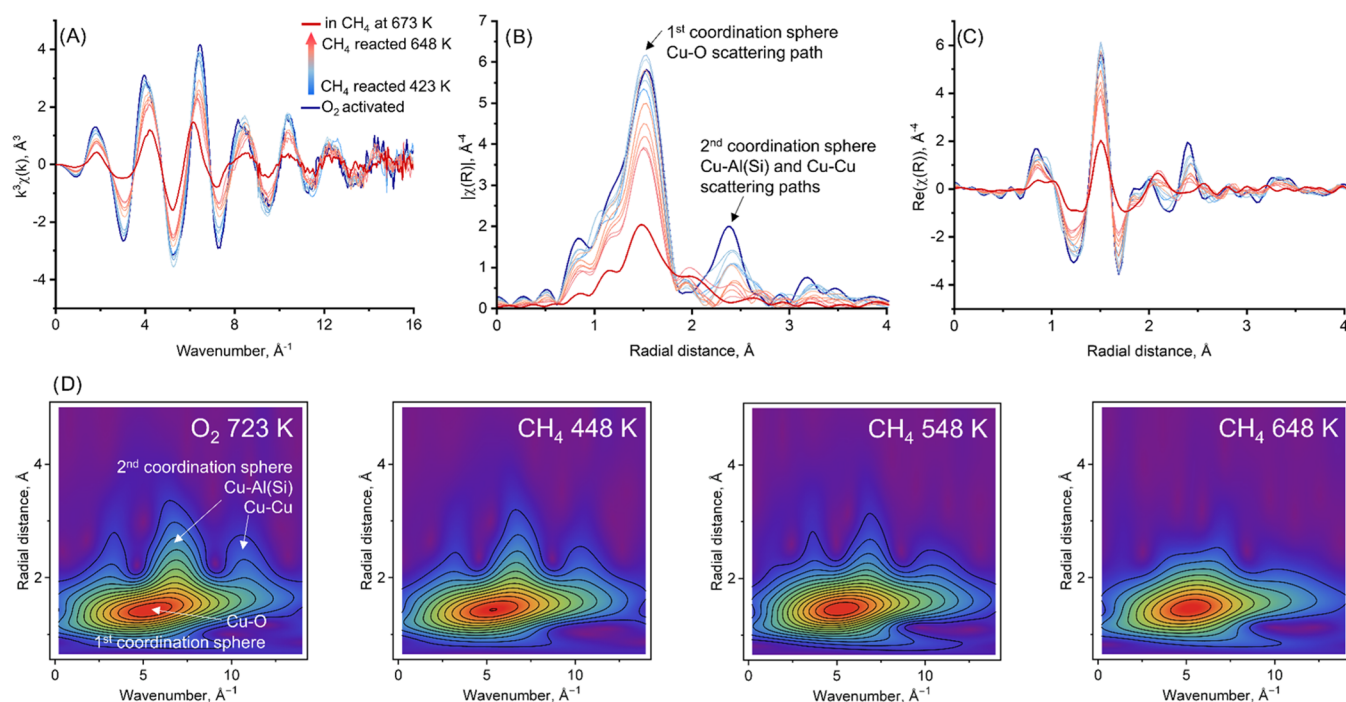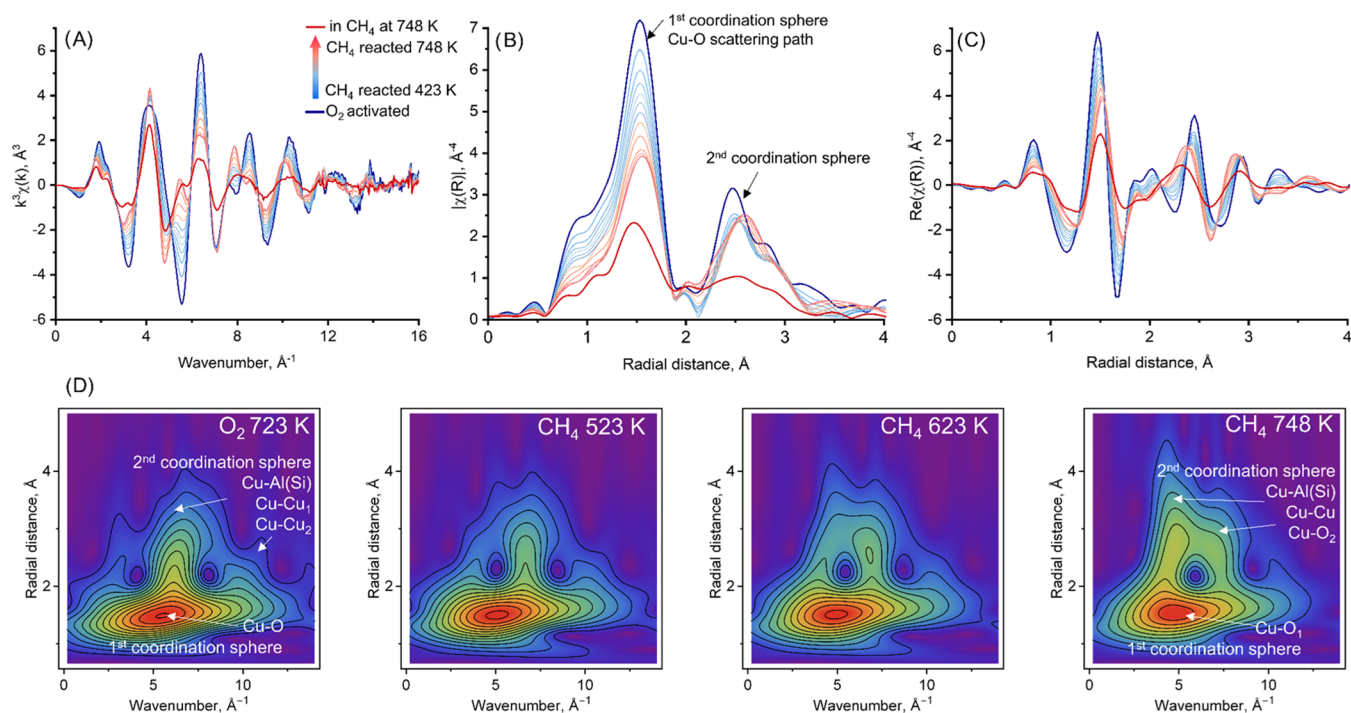
Figure 5. k^3-weighted $\chi(k)$ spectra (A) and the corresponding phase-uncorrected magnitude (B) and real part (C) of Fourier transform and contour plots of wavelet transform (D) acquired at different stages of the reaction between CuFAU material with methane. The spectra shown in blue thick lines correspond to oxygen-activated CuFAU and are acquired at ambient temperature, the spectra shown in thin lines are related to the state of the material after the reaction with methane at various temperatures and are acquired at ambient temperature, and the spectra shown in red thick lines correspond to the highest reaction temperature with acquisition at 748 K without cooling.

reaction temperature leads to an overall decrease in the intensity of oscillations in k-space in the range between 2 and 10 Å^{-1} without affecting their position. At the same time, in the region between 10 and 16 Å^{-1}, slight shift of the location corresponding to minima and maxima of oscillations is observed. In the phase-uncorrected FT EXAFS spectra, there are two peaks at radial distances of about 1.5 and 2.3 Å. The first peak is due to oxygen atoms in the first coordination sphere and the second peak originates from the interference of scattered waves from silicon or aluminum atoms in the zeolite framework and extra-framework copper atoms.[10,17,20,47,68] The reaction of CuMFI and CuMOR with methane leads to the gradual decrease of intensity of the first peak and almost complete disappearance of the second peak. Analysis of WT spectra reveals similar results: after activation in oxygen, the spectra contain pronounced lobes at (7 Å^{-1}; 2.4 Å) and (12 Å^{-1}; 2.3 Å), that diminish upon a reaction with methane (Figures 3D and 4D and Movies S1 and S2).

Notably, the evolution of the spectra corresponding to the CuFAU material is completely different (Figure 5). The reaction with methane leads to significant changes in the entire range of k-space. The intensity of oscillations having their minimum at 5.6 Å^{-1} and maximum at 6.5 Å^{-1} significantly decreases, while a new oscillation possessing a minimum 4.9 Å^{-1} and a maximum at 5.6 Å^{-1} develops in the spectra. Similarly to the evolution of the XANES spectra of CuFAU (Figure 2C), the k^3-weighted $\chi(k)$ spectra corresponding to different stages of the reaction possess isosbestic points. In the course of the reaction, the intensity of the first peak in the magnitude of Fourier transform decreases, and the position of the maximum shifts from 1.55 to 1.60 Å. The second peak undergoes significant changes as well: the shape transforms from a peak having a maximum at 2.47 Å

with a clear shoulder at 2.85 Å to an asymmetric one centered at 2.64 Å. The wavelet transforms show significant changes in the signals due to the second coordination sphere (Figure 5D and Movie S3): for the oxygen-activated sample, the main signal originates from an intense and pronounced lobe at (6 Å^{-1}; 2.8 Å) and additional weak lobes at (3 Å^{-1}; 2.6 Å) and (11 Å^{-1}; 2.6 Å). The reaction with methane leads to a decrease in the intensity of the lobe at (6 Å^{-1}; 2.8 Å) and the appearance of a signal at (5 Å^{-1}; 3 Å), dominating at the final stage of the reaction between CuFAU and methane.

3.3. EXAFS Fitting: CuMOR and CuMFI. Quantitative information about the structure of the copper sites and their evolution in the course of the reaction with methane was obtained by fitting of the EXAFS data. To monitor the evolution of the structure of copper sites in the course of the chemical reaction and exclude any effects due to the temperature variation, we performed the analysis using the data acquired at ambient temperature. Moreover, the structure at high temperature generally demonstrates higher degree of disorder, resulting in higher values of the Debye−Waller factor,[75] hence complicating the interpretation; in the case of CuFAU, even causing the fitting to not to converge. Therefore, we have limited the analysis of the spectra, acquired at high temperature, to the fitting of only first coordination sphere.

The reduction of copper(II) sites in MOR and MFI zeolites leads to a decrease of the intensity of the signals in both first and second coordination spheres, without the appearance of signals due to additional scattering paths.[20,47,50] The reaction with methane leads to the formation of copper(I) carbonyl species.[21,75,76] We quantified the amount of these copper species by means of *in situ* Fourier transform infrared (FTIR) spectroscopy, given recently reported attenuation coefficient,[77]
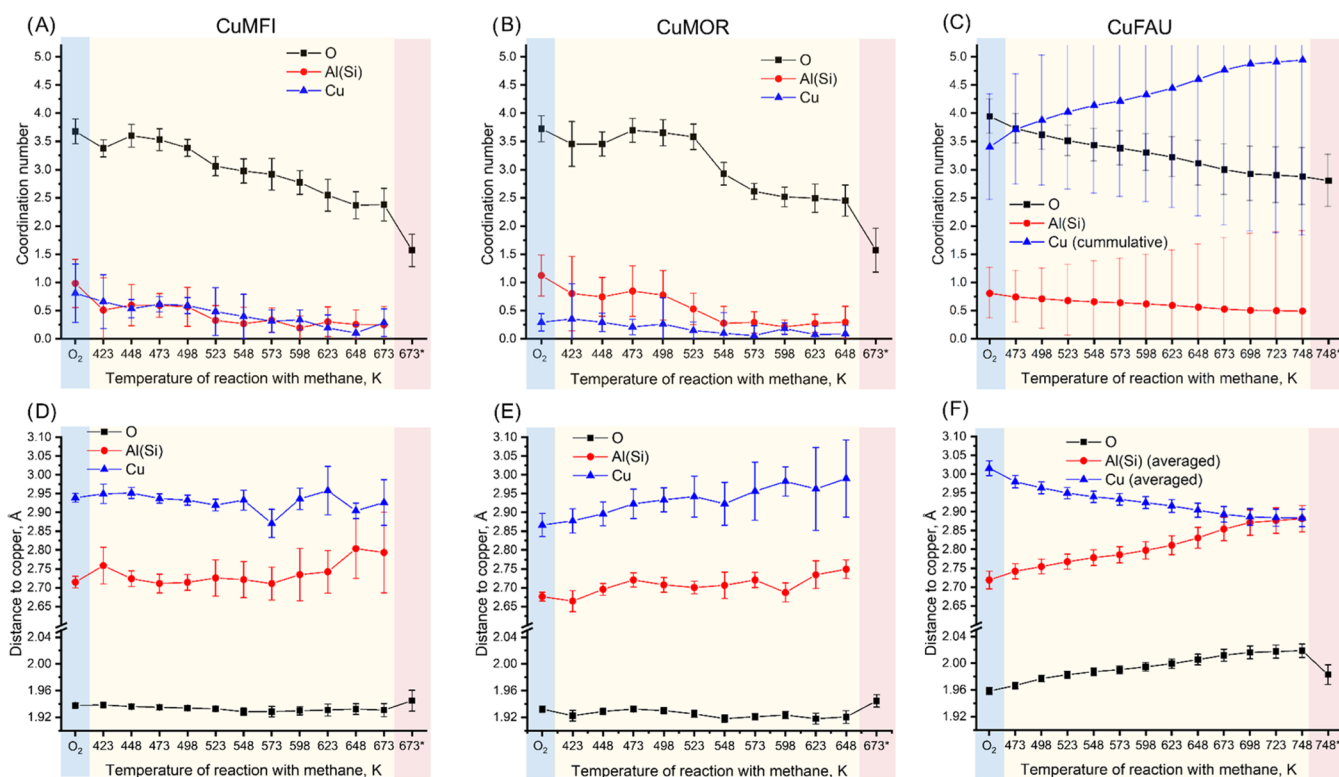
Figure 6. Coordination numbers (A−C) and the distances to corresponding scatterers (D−F) providing the best fit for the k^3-weighted EXAFS spectra at different stages of the reaction with methane for CuMFI, CuMOR, and CuFAU, respectively. The data highlighted in blue correspond to oxygen-activated materials, the data highlighted in yellow are related to the state of the materials after the reaction with methane at various temperatures and spectra acquisition at ambient temperature, and the data highlighted in red and marked with asterisks are acquired exactly at the corresponding temperature with no cooling.

and found that their overall fraction is not more than 7% for all studied materials even at the highest reaction temperature (Figure S1 and Table S1). Moreover, modeling of the EXAFS spectra of these centers predicts pronounced characteristic signals in the second coordination sphere; such features were not observed in the experimental spectra of materials after the reaction with methane (Figure S2). Based on this, we conclude that copper(I) carbonyls represent the minority of species, and the model comprising Cu−O, Cu−Si/Al, and Cu−Cu scattering paths was used as an initial guess for fitting of EXAFS data corresponding to CuMFI and CuMOR materials before and after the reaction with methane. Figure 6 and Tables S2 and S3 summarize the fitting results corresponding to CuMFI and CuMOR samples; the comparison of experimental and fitted data are shown in Figures S6−S18 for CuMFI and S19−S30 for CuMOR, respectively. In line with the selected model, the peak in the first shell originates exclusively from oxygen atoms; the fitting of this region is straightforward. For the oxygen-activated CuMFI and CuMOR, the distance to oxygen atoms corresponds to 1.94 ± 0.01 and 1.93 ± 0.01 Å, and the coordination number is 3.6 ± 0.3, respectively, in line with literature data reported for these systems.[25,73,78−80] The progressive reaction with methane does not significantly affect the distance between copper and oxygen atoms. At the same time, a gradual decrease in the coordination numbers to 2.4 ± 0.3 and 2.5 ± 0.3 for CuMFI and CuMOR, respectively, was observed, indicating the removal of the extra-framework oxygen from the copper sites. The values of the coordination number due to oxygen atoms and the distance to copper are similar to that reported for copper(I)-containing MFI and MOR materials,[71−73] confirming close to complete

reduction of copper(II) sites into copper(I). Interestingly, the fitting of the spectra acquired in methane at 673 K gives even lower values of the coordination number, namely, 1.6 ± 0.3 for CuMFI and 1.7 ± 0.5 for CuMOR, respectively.

The fitting of the second coordination shell is more challenging due to the contribution from at least two scatterers—framework silicon or aluminum atoms and extra-framework copper (Figure S5). The distances to the aluminum/silicon and copper scatterers in the oxygen-activated CuMFI were 2.71 ± 0.02 and 2.94 ± 0.01 Å, and corresponding coordination numbers were 1.0 ± 0.4 and 0.8 ± 0.5, respectively. For the oxygen-activated CuMOR, fitting reveals the distance to the aluminum/silicon and copper atoms of 2.68 ± 0.01 and 2.87 ± 0.01 Å, respectively, with corresponding coordination numbers of 1.1 ± 0.4 and 0.3 ± 0.2, respectively.

3.4. EXAFS Fitting: The CuFAU Case. The reaction of CuFAU with methane leads to drastic changes in EXAFS. Notably, the XANES and EXAFS spectra contain pronounced isosbestic points (Figures 2C and 5), indicating that each spectrum in between can be described as a linear combination of spectra corresponding to the initial, Cu^{II}FAU and final, Cu^{I}FAU, ones. Both Cu^{II}FAU and Cu^{I}FAU spectra contain pronounced signals in the second coordination sphere (Figure 5B,C), yet significantly different wavelet transform maps (Figure 5D) indicate that the reduction leads to the rearrangement in the second sphere. Therefore, two independent models should be developed to fit these two states corresponding to copper(II) and copper(I) sites in CuFAU.

The pronounced signals in the second coordination sphere shell of FT of Cu^{II}FAU and Cu^{I}FAU EXAFS spectra (Figure

5B,C) and the presence of lobes located in the region of $k > 10$ Å^{-1} in WT spectra (Figure 5D and Movie S3) indicate the possible contribution from Cu−Cu scattering paths. In this respect, the comparison with the bulk copper(II) and copper(I) oxides helps in the development of the models. Figure S34A,B compares the real part of FT and the WT of k^3-weighted EXAFS data of Cu^{I}FAU, Cu^{II}FAU, and bulk copper(I) and copper(II) oxides.

The comparison of the WT spectra corresponding to bulk copper(II) oxide and Cu^{II}FAU shows similarities: in both cases, there is an intense lobe at (6 Å^{-1}; 3 Å) and a lobe at (12 Å^{-1}; 3 Å), indicating significant contribution to the second coordination sphere from Cu−Cu scattering paths. However, the shape of the real part, as well as the relative intensities of lobes in the WT are different. Therefore, the structure of the bulk copper(II) oxide can not be directly used as an initial guess for the fitting of the Cu^{II}FAU spectrum. In this respect, a DFT-optimized model of copper oxide Cu$_8^{II}$O$_6^{4+}$ cluster hosted in the FAU supercage was used.[17] This model accounts for the presence of copper(II) sites preferably in a form of aggregated copper(II)-oxo species, and at the same time, takes into account possible confinement effects of the zeolite framework on the structure of copper(II)-oxo cluster. Figure S31 shows the fitting of experimental data for Cu^{II}FAU after the oxygen pretreatment, and the best fit parameters are summarized in Table S4. According to the utilized model, the signal in the first coordination sphere is due to the copper−oxygen scattering path with oxygen atoms at the distance of 1.96 ± 0.01 Å having a coordination number of 3.9 ± 0.3. The signal in the second coordination sphere has overlapping contributions from aluminum (and/or silicon) and two distinct copper scatterers, with distances to the absorbing atom equal to 2.73 ± 0.02, 2.94 ± 0.02, and 3.09 ± 0.01 Å and corresponding coordination numbers of 0.8 ± 0.3, 1.7 ± 0.6, and 1.7 ± 0.7, respectively. The cumulative coordination number of copper scatterers for oxygen-activated CuFAU calculated as a sum of individual copper scatterers was equal to 3.4 ± 1.0. This value was used only for the comparison with the model describing Cu^{I}FAU (*vide infra*).

The comparison of the data for copper(I) oxide and Cu^{I}FAU shows that the shape of the Cu^{I}FAU signal in the region of 2.0−3.3 Å in real space of FT resembles that of cuprite. Moreover, the part of the WT spectra corresponding to the second coordination sphere for copper(I) oxide and Cu^{I}FAU look similar: there is a pronounced lobe at (6 Å^{-1}; 3 Å) and an additional weak lobe at (8 Å^{-1}; 3 Å). The fitting of the data acquired for bulk copper(I) oxide using the crystal structure of cuprite shows that the signal in the second coordination sphere originates from Cu−Cu and Cu−O scattering pathways (Figure S35 and Table S6). Based on that, for the fitting of Cu^{I}FAU, we employed the model with the following scattering paths: Cu−O in the first coordination sphere and Cu−Al(Si), Cu−Cu, and Cu−O in the second coordination sphere (Figure S5). The aluminum (and/or silicon) scatterers in the second coordination sphere were added to account for the zeolite framework surrounding cuprous oxide cluster. Figure S32 and Table S4 summarize the results of the fitting for Cu^{I}FAU spectrum. The signal in the first coordination sphere originates from the oxygen atoms at a distance of 2.01 ± 0.01 Å with a coordination number of 2.8 ± 0.5. The signal in the second coordination sphere is represented by a superposition of aluminum (silicon), copper, and oxygen scatterers located at distances 2.87 ± 0.03, 2.88 ± 0.02, and 3.37 ± 0.04 Å from the absorbing copper atom and having coordination numbers of 0.5 ± 1.1, 4.9 ± 3.2, and 3.2 ±

1.2, respectively. Calculations show that during the restructuring, the coordination number due to aluminum/silicon gradually decreases, while the corresponding distance increases. In contrast, the cumulative copper coordination numbers increase, accompanied by the decreasing averaged distance to copper.

The results of linear combination fitting of the EXAFS spectra corresponding to CuFAU at the different stages of the reaction with methane using Cu^{I}FAU and Cu^{II}FAU components are presented in Table S5 and Figure S33. The approach provides a close match of the experimental spectra with the one obtained as linear combination, and fitting results show that the contribution from Cu^{I}FAU gradually increases from 0.2 to 1, indicating transformation of copper(II) sites into copper(I) species. Notably, the fraction of copper(I) determined using LCF of XANES (Figure S4) is very close to the fraction of the Cu^{I}FAU component extracted from LCF of EXAFS spectra (Figure S33).

4. DISCUSSION

The analysis of XANES and EXAFS provides complementary information on the oxidation state of copper atoms and their local environment after oxidative activation and a subsequent reaction with methane, allowing tracking the evolution of different copper sites. The reduction of copper(II) sites with methane leads to the formation of exclusively copper(I) sites, and no metallic copper(0) is formed even at temperatures as high as 748 K. This is important for repetitive methane conversion to methanol *via* chemical looping, since the reduction to metallic copper is a partially irreversible process,[35] while copper(I) sites can be easily reoxidized into copper(II) species.[48,49,57] The XANES spectra of oxygen-activated CuMFI and CuMOR materials look similar, while the spectrum of oxygen-activated CuFAU differs from them (Figure S3) due to distinct coordination of ligands around copper atoms.[17] The difference between CuMFI/CuMOR and CuFAU becomes even more pronounced when the spectra corresponding to the final stage of the reaction with methane are compared (Figure S3). This indicates that the zeolite framework significantly affects the nature of copper(II) species present in the oxygen-activated material, as well as that of the structure of copper(I) sites formed by the reduction with methane.

Copper atoms in oxygen-activated CuMFI, CuMOR, and CuFAU are surrounded with four oxygen scattering atoms in the first coordination sphere (Figure 6A−C and Tables S2−S4). The gradual reduction of copper(II) sites leads to a gradual decrease in the oxygen coordination number. This is in line with the loss of extra-framework oxygen upon reduction of copper(II) sites, which has been shown in numerous studies.[20,23,47,50,73] Interestingly, the loss of oxygen in the first sphere for CuFAU is less pronounced than in those of CuMFI and CuMOR (Figure 6A−C). Thus, in the spectra acquired at the highest reaction temperature, the oxygen coordination number for CuFAU stays above 2.5 ± 0.5, while for CuMFI and CuMOR, it drops to 1.7 ± 0.3. The higher coordination number observed for CuFAU suggests that copper atoms still partially coordinate extra-framework oxygen. Notably, for CuMFI and CuMOR, the copper reduction has no significant effect on the Cu−O interatomic distance in the first coordination sphere, while in the case of CuFAU, the average distance to oxygen scatterers increases due to the formation of other type of copper(I) sites.

The results of the fitting of the second coordination sphere provides additional information on the copper speciation. For
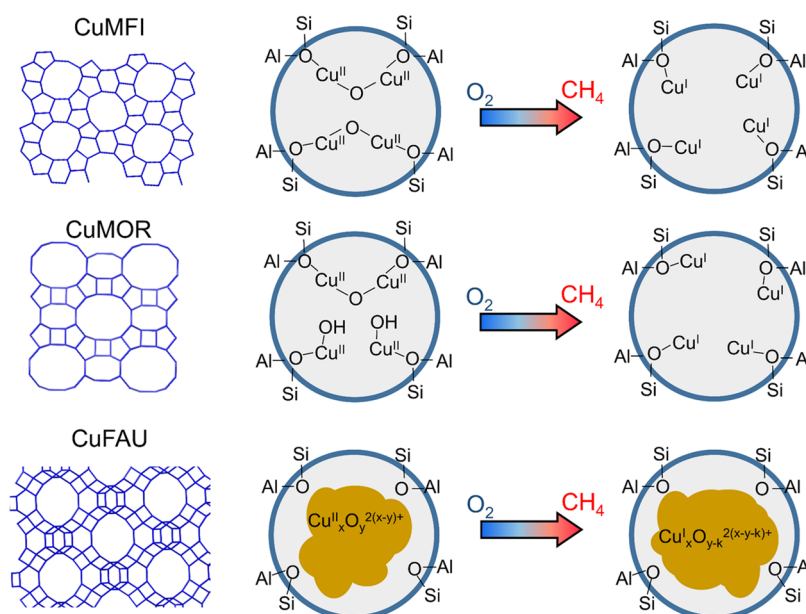
Figure 7. Structures of different copper sites hosted in zeolites of various framework types and their evolution during the reaction with methane.

oxygen-activated CuMFI material, the coordination number for both aluminum (and/or silicon) and copper scatterers in the second coordination sphere is close to one, suggesting the presence of mostly dimeric copper sites, in line with previous reports.[8,17,81] For activated CuMOR material, the optimized Cu−Cu coordination number is 0.3, significantly lower than 1, indicating the presence of a significant fraction of copper monomeric species in addition to copper dimeric sites.[17,19,20,23,81] Different copper speciation in MOR and MFI materials is apparently the result of the zeolite framework confinement effect and, possibly, different copper loadings and Si/Al ratios. Notably, the Cu−Al and Cu−Cu interatomic distances are slightly different for CuMFI and CuMOR, indicating different geometry of mono-μ-oxo copper dimers due to the effect of the zeolite framework, confirmed by DFT studies.[82] While the presence of trimeric copper-oxo species was reported for copper-containing mordenite,[31] we did not observe any spectroscopic signatures of these centers (presence of scattering paths due to copper scatterers located at a distance above 3 Å) in the studied oxygen-activated CuMOR material. This may be associated with the utilization of different parent zeolites and synthetic protocols. The reaction of CuMFI and CuMOR with methane leads to similar gradual changes in the second coordination sphere. The progressive reaction with methane leads to the gradual decline of the amplitudes corresponding to both scattering paths in the second shell, albeit without a prominent effect on the position of aluminum and copper scattering atoms. After the reaction with methane (Figures S17 and S29), the peak due to the second shell is almost absent, resembling data for MOR and MFI materials containing exclusively cationic Cu[I] sites prepared *via* gas-phase exchange between zeolites in proton form and CuCl.[71−73] The results are in line with the presence of the signal in the second coordination sphere in FT EXAFS of copper(II)-containing MFI and the absence of the corresponding signal in the spectra of copper(I)-containing MFI reported by Palomino et al.[73] Lomachenko et al.[20] and Deplano et al.[50] recently demonstrated that the reduction of a substantial fraction of copper(II) sites in CuMOR leads to a similar trend of vanishing of the signal in the second

coordination sphere. The decrease of coordination numbers of scattering atoms in the second coordination sphere for CuMOR and CuCHA was also reported by Borfecchia et al.[47] Notably, in the mentioned studies, only a partial decrease of the intensity of the signals in the second coordination sphere was observed, possibly due to incomplete reduction of copper(II) sites with methane. We demonstrate that the complete reduction of copper(II) dimeric sites with methane leads to total conversion of the dicopper cores into isolated Cu[I] sites, apparently existing in a cationic form balancing the charge in the zeolite framework.

A significantly different speciation of both copper(II) and copper(I) sites was observed for CuFAU. First, the FAU framework stabilizes aggregated copper(II)-oxo clusters after the oxidative pretreatment.[17] In the course of the reaction with methane, the presence of the pronounced signal in the second coordination sphere is preserved, yet the nature of the scatterers, their positions, and their coordination numbers change dramatically, hence indicating significant restructuring of the copper-oxo clusters. The structure of these reduced copper(I)-oxo clusters resembles that of bulk copper(I) oxide, yet the zeolite framework and the presence of charged aluminum on ion-exchange positions affect the interatomic distances. Interestingly, the observed presence of copper(I)-oxo clusters in CuFAU after a reaction with methane is completely different from the copper(I) speciation for CuFAU prepared *via* a reaction between the proton form of the parent zeolite and gaseous CuCl, where isolated copper(I) cations constitute the majority of sites.[83,84] This shows that the nature of the hosted copper(I) sites in zeolitic materials depends not only on the properties of the zeolite host but also is a function of the preparation method.

Figure 7 summarizes the structures of copper species in different zeolites and their evolution in the course of the reaction with methane. First, the zeolite framework significantly affects the nature of the copper(II) sites formed after activation pretreatment in oxygen. For CuMFI, mono-μ-oxo dicopper(II) sites are major type of copper centers and for CuMOR, there is a combination of dimeric and monomeric copper(II) sites and CuFAU hosts copper(II)-oxo clusters. In turn, the reduction of

different copper(II) sites leads to formation of different copper(I) species. Copper(II) monomeric and dimeric centers are both transformed into isolated copper(I) cationic sites. The copper(II)-oxo clusters in the course of reduction with methane are restructured, forming copper(I)-oxo clusters.

5. CONCLUSIONS

Cu K-edge XANES and EXAFS identified the oxidation state and the local environment of copper atoms in copper-containing MFI, MOR, and FAU zeolites. Oxygen-activated materials contain copper(II)-oxo sites, which are gradually reduced to copper(I) species in the course of the reaction with methane; no formation of metallic copper has been observed up to 748 K. The nature of formed copper(I) sites is governed by the structure of copper(II) sites, which, in turn, is defined by the zeolite framework. Dimeric and monomeric copper(II) sites hosted in the MFI and MOR framework are reduced to copper(I) cationic species. In contrast, copper(II)-oxo clusters stabilized in CuFAU undergo restructuring upon the reduction with formation of copper(I)-oxo clusters having a structure resembling that of bulk copper(I) oxide. The findings will aid in the fundamental understanding of the process of methane oxidation over different copper(II) active sites at the molecular level.

ASSOCIATED CONTENT

ⓢ Supporting Information

The Supporting Information is available free of charge at https://pubs.acs.org/doi/10.1021/acs.jpcc.3c01496.

> In situ FTIR spectroscopy for quantification of copper(I) carbonyl species, modeling of EXAFS spectra of copper-(I) carbonyl species, comparison of XANES spectra of oxygen-activated and methane-reacted materials, EXAFS fitting results for CuMFI and CuMOR, and results of LCF of CuFAU and fitting of EXAFS spectrum of copper(I) oxide (PDF)
>
> Demonstration of wavelet transformation of Cu K-edge EXAFS spectra corresponding to CuMFI after activation in oxygen and a subsequent reaction with methane at different temperatures (Movie_S1_CuMFI.mp4) (MP4)
>
> Demonstration of wavelet transformation of Cu K-edge EXAFS spectra corresponding to CuMOR after activation in oxygen and a subsequent reaction with methane at different temperatures (Movie_S2_CuMOR.mp4) (MP4)
>
> Demonstration of wavelet transformation of Cu K-edge EXAFS spectra corresponding to CuFAU after activation in oxygen and a subsequent reaction with methane at different temperatures (Movie_S3_CuFAU.mp4) (MP4)

AUTHOR INFORMATION

Corresponding Authors

Jeroen A. van Bokhoven − *Institute for Chemistry and Bioengineering, ETH Zurich, 8093 Zurich, Switzerland; Laboratory for Catalysis and Sustainable Chemistry, Paul Scherrer Institute, 5232 Villigen PSI, Switzerland;* ⓘ orcid.org/0000-0002-4166-2284; Email: jeroen.vanbokhoven@chem.ethz.ch

Vitaly L. Sushkevich − *Laboratory for Catalysis and Sustainable Chemistry, Paul Scherrer Institute, 5232 Villigen PSI, Switzerland;* ⓘ orcid.org/0000-0002-3788-8969; Phone: +41563103518; Email: vitaly.sushkevich@psi.ch

Authors

Mikalai A. Artsiusheuski − *Institute for Chemistry and Bioengineering, ETH Zurich, 8093 Zurich, Switzerland; Laboratory for Catalysis and Sustainable Chemistry, Paul Scherrer Institute, 5232 Villigen PSI, Switzerland;* ⓘ orcid.org/0000-0003-4931-9568

Olga Safonova − *Laboratory for Operando Spectroscopy, Paul Scherrer Institute, 5232 Villigen PSI, Switzerland;* ⓘ orcid.org/0000-0002-6772-1414

Dennis Palagin − *Delft High Performance Computing Centre, Delft University of Technology, 2628 CD Delft, The Netherlands;* ⓘ orcid.org/0000-0001-5251-3471

Complete contact information is available at: https://pubs.acs.org/10.1021/acs.jpcc.3c01496

Notes

The authors declare no competing financial interest.

REFERENCES

(1) Li, Y.; Hall, W. K. Catalytic Decomposition of Nitric Oxide over Cu-Zeolites. *J. Catal.* **1991**, *129*, 202−215.

(2) Zhang, W. X.; Yahiro, H.; Mizuno, N.; Izumi, J.; Iwamoto, M. Removal of Nitrogen Monoxide on Copper Ion-Exchanged Zeolites by Pressure Swing Adsorption. *Langmuir* **1993**, *9*, 2337−2343.

(3) Smeets, P. J.; Groothaert, M. H.; van Teeffelen, R. M.; Leeman, H.; Hensen, E. J. M.; Schoonheydt, R. A. Direct NO and N2O Decomposition and NO-Assisted N2O Decomposition over Cu-Zeolites: Elucidating the Influence of the Cu-Cu Distance on Oxygen Migration. *J. Catal.* **2007**, *245*, 358−368.

(4) Vennestrøm, P. N. R.; Thøgersen, J. R.; Gabrielsson, P. L. T.; van Tendeloo, L.; Schütze, F.-W.; Moliner, M. Advances and Perspectives from a Decade of Collaborative Efforts on Zeolites for Selective Catalytic Reduction of NOx. *Microporous Mesoporous Mater.* **2022**, No. 112336.

(5) Xin, Y.; Li, Q.; Zhang, Z. Zeolitic Materials for DeNOx Selective Catalytic Reduction. *ChemCatChem* **2018**, *10*, 29−41.

(6) Kumar, M. S.; Alphin, M. S.; Kumar, P. S.; Raja, S. A Review on Zeolite Catalyst for DeNOx Performance in Ammonia−Selective Catalytic Reduction. *Fuel* **2023**, *334*, No. 126828.

(7) Groothaert, M. H.; Smeets, P. J.; Sels, B. F.; Jacobs, P. A.; Schoonheydt, R. A. Selective Oxidation of Methane by the Bis(μ-Oxo)Dicopper Core Stabilized on ZSM-5 and Mordenite Zeolites. *J. Am. Chem. Soc.* **2005**, *127*, 1394−1395.

(8) Woertink, J. S.; Smeets, P. J.; Groothaert, M. H.; Vance, M. A.; Sels, B. F.; Schoonheydt, R. A.; Solomon, E. I. A [Cu2O]2+ Core in Cu-ZSM-5, the Active Site in the Oxidation of Methane to Methanol. *Proc. Natl. Acad. Sci. U.S.A.* **2009**, *106*, 18908−18913.

(9) Tomkins, P.; Ranocchiari, M.; van Bokhoven, J. A. Direct Conversion of Methane to Methanol under Mild Conditions over Cu-Zeolites and Beyond. *Acc. Chem. Res.* **2017**, *50*, 418−425.

(10) Pappas, D. K.; Borfecchia, E.; Dyballa, M.; Pankin, I. A.; Lomachenko, K. A.; Martini, A.; Signorile, M.; Teketel, S.; Arstad, B.; Berlier, G.; et al. Methane to Methanol: Structure-Activity Relationships for Cu-CHA. *J. Am. Chem. Soc.* **2017**, *139*, 14961−14975.

(11) Narsimhan, K.; Iyoki, K.; Dinh, K.; Román-Leshkov, Y. Catalytic Oxidation of Methane into Methanol over Copper-Exchanged Zeolites with Oxygen at Low Temperature. *ACS Cent. Sci.* **2016**, *2*, 424−429.

(12) Newton, M. A.; Knorpp, A. J.; Sushkevich, V. L.; Palagin, D.; van Bokhoven, J. A. Active Sites and Mechanisms in the Direct Conversion of Methane to Methanol Using Cu in Zeolitic Hosts: A Critical Examination. *Chem. Soc. Rev.* **2020**, *49*, 1449−1486.

(13) Smeets, P. J.; Groothaert, M. H.; Schoonheydt, R. A. Cu Based Zeolites: A UV-Vis Study of the Active Site in the Selective Methane Oxidation at Low Temperatures. *Catal. Today* **2005**, *110*, 303−309.

(14) Pappas, D. K.; Martini, A.; Dyballa, M.; Kvande, K.; Teketel, S.; Lomachenko, K. A.; Baran, R.; Glatzel, P.; Arstad, B.; Berlier, G.; et al. The Nuclearity of the Active Site for Methane to Methanol Conversion in Cu-Mordenite: A Quantitative Assessment. *J. Am. Chem. Soc.* **2018**, *140*, 15270−15278.

(15) Sushkevich, V. L.; Smirnov, A. V.; van Bokhoven, J. A. Autoreduction of Copper in Zeolites: Role of Topology, Si/Al Ratio, and Copper Loading. *J. Phys. Chem. C* **2019**, *123*, 9926−9934.

(16) Sushkevich, V. L.; van Bokhoven, J. A. Methane-to-Methanol: Activity Descriptors in Copper-Exchanged Zeolites for the Rational Design of Materials. *ACS Catal.* **2019**, *9*, 6293−6304.

(17) Sushkevich, V. L.; Safonova, O. V.; Palagin, D.; Newton, M. A.; van Bokhoven, J. A. Structure of Copper Sites in Zeolites Examined by Fourier and Wavelet Transform Analysis of EXAFS. *Chem. Sci.* **2020**, *11*, 5299−5312.

(18) Rhoda, H. M.; Plessers, D.; Heyer, A. J.; Bols, M. L.; Schoonheydt, R. A.; Sels, B. F.; Solomon, E. I. Spectroscopic Definition of a Highly Reactive Site in Cu-CHA for Selective Methane Oxidation: Tuning a Mono-μ-Oxo Dicopper(II) Active Site for Reactivity. *J. Am. Chem. Soc.* **2021**, *143*, 7531−7540.

(19) Sushkevich, V. L.; Palagin, D.; van Bokhoven, J. A. The Effect of the Active-Site Structure on the Activity of Copper Mordenite in the Aerobic and Anaerobic Conversion of Methane into Methanol. *Angew. Chem., Int. Ed.* **2018**, *57*, 8906−8910.

(20) Lomachenko, K. A.; Martini, A.; Pappas, D. K.; Negri, C.; Dyballa, M.; Berlier, G.; Bordiga, S.; Lamberti, C.; Olsbye, U.; Svelle, S.; et al. The Impact of Reaction Conditions and Material Composition on the Stepwise Methane to Methanol Conversion over Cu-MOR: An Operando XAS Study. *Catal. Today* **2019**, *336*, 99−108.

(21) Sushkevich, V. L.; Verel, R.; van Bokhoven, J. A. Pathways of Methane Transformation over Copper-Exchanged Mordenite as Revealed by In Situ NMR and IR Spectroscopy. *Angew. Chem.* **2020**, *132*, 920−928.

(22) Knorpp, A. J.; Pinar, A. B.; Newton, M. A.; Sushkevich, V. L.; van Bokhoven, J. A. Copper-Exchanged Omega (MAZ) Zeolite: Copper-Concentration Dependent Active Sites and Its Unprecedented Methane to Methanol Conversion. *ChemCatChem* **2018**, *10*, 5593−5596.

(23) Sushkevich, V. L.; Artsiusheuski, M.; Klose, D.; Jeschke, G.; van Bokhoven, J. A. Identification of Kinetic and Spectroscopic Signatures of Copper Sites for Direct Oxidation of Methane to Methanol. *Angew. Chem., Int. Ed.* **2021**, *60*, 15944−15953.

(24) Grundner, S.; Luo, W.; Sanchez-Sanchez, M.; Lercher, J. A. Synthesis of Single-Site Copper Catalysts for Methane Partial Oxidation. *Chem. Commun.* **2016**, *52*, 2553−2556.

(25) Brezicki, G.; Zheng, J.; Paolucci, C.; Schlögl, R.; Davis, R. J. Effect of the Co-Cation on Cu Speciation in Cu-Exchanged Mordenite and ZSM-5 Catalysts for the Oxidation of Methane to Methanol. *ACS Catal.* **2021**, *11*, 4973−4987.

(26) Heyer, A. J.; Plessers, D.; Braun, A.; Rhoda, H. M.; Bols, M. L.; Hedman, B.; Hodgson, K. O.; Schoonheydt, R. A.; Sels, B. F.; Solomon, E. I. Methane Activation by a Mononuclear Copper Active Site in the Zeolite Mordenite: Effect of Metal Nuclearity on Reactivity. *J. Am. Chem. Soc.* **2022**, *144*, 19305−19316.

(27) Vanelderen, P.; Snyder, B. E. R.; Tsai, M. L.; Hadt, R. G.; Vancauwenbergh, J.; Coussens, O.; Schoonheydt, R. A.; Sels, B. F.; Solomon, E. I. Spectroscopic Definition of the Copper Active Sites in Mordenite: Selective Methane Oxidation. *J. Am. Chem. Soc.* **2015**, *137*, 6383−6392.

(28) Artsiusheuski, M. A.; Van Bokhoven, J. A.; Sushkevich, V. L. Structure of Selective and Nonselective Dicopper (II) Sites in CuMFI for Methane Oxidation to Methanol. *ACS Catal.* **2022**, *12*, 15626−15637.

(29) Groothaert, M. H.; van Bokhoven, J. A.; Battiston, A. A.; Weckhuysen, B. M.; Schoonheydt, R. A. Bis(μ-Oxo)Dicopper in Cu-ZSM-5 and Its Role in the Decomposition of NO: A Combined in Situ XAFS, UV-Vis-near-IR, and Kinetic Study. *J. Am. Chem. Soc.* **2003**, *125*, 7629−7640.

(30) Ipek, B.; Wulfers, M. J.; Kim, H.; Göltl, F.; Hermans, I.; Smith, J. P.; Booksh, K. S.; Brown, C. M.; Lobo, R. F. Formation of [Cu2O2]2+ and [Cu2O]2+ toward C-H Bond Activation in Cu-SSZ-13 and Cu-SSZ-39. *ACS Catal.* **2017**, *7*, 4291−4303.

(31) Grundner, S.; Markovits, M. A. C.; Li, G.; Tromp, M.; Pidko, E. A.; Hensen, E. J. M.; Jentys, A.; Sanchez-Sanchez, M.; Lercher, J. A. Single-Site Trinuclear Copper Oxygen Clusters in Mordenite for Selective Conversion of Methane to Methanol. *Nat. Commun.* **2015**, *6*, No. 7546.

(32) Markovits, M. A. C.; Jentys, A.; Tromp, M.; Sanchez-Sanchez, M.; Lercher, J. A. Effect of Location and Distribution of Al Sites in ZSM-5 on the Formation of Cu-Oxo Clusters Active for Direct Conversion of Methane to Methanol. *Top. Catal.* **2016**, *59*, 1554−1563.

(33) Palagin, D.; Knorpp, A. J.; Pinar, A. B.; Ranocchiari, M.; van Bokhoven, J. A. Assessing the Relative Stability of Copper Oxide Clusters as Active Sites of a CuMOR Zeolite for Methane to Methanol Conversion: Size Matters. *Nanoscale* **2017**, *9*, 1144−1153.

(34) Kolganov, A. A.; Gabrienko, A. A.; Yashnik, S. A.; Pidko, E. A.; Stepanov, A. G. Nature of the Surface Intermediates Formed from Methane on Cu-ZSM-5 Zeolite: A Combined Solid-State Nuclear Magnetic Resonance and Density Functional Theory Study. *J. Phys. Chem. C* **2020**, *124*, 6242−6252.

(35) Herman, R. G.; Lunsford, J. H.; Beyer, H.; Jacobs, P. A.; Uytterhoeven, J. B. Redox Behavior of Transition Metal Ions in Zeolites. I. Study of the Reversibility of the Hydrogen Reduction of Copper Y Zeolites. *J. Phys. Chem.* **1975**, *79*, 2388−2394.

(36) Song, H.; Chang, Y.; Wan, X.; Dai, M.; Song, H.; Jin, Z. Equilibrium, Kinetic, and Thermodynamic Studies on Adsorptive Desulfurization onto CuICeIVY Zeolite. *Ind. Eng. Chem. Res.* **2014**, *53*, 5701−5708.

(37) Texter, J.; Strome, D. H.; Herman, R. G.; Klier, K. Chemical and Spectroscopic Properties of Copper Containing Zeolites. *J. Phys. Chem.* **1977**, *81*, 333−338.

(38) Wang, H.; Xu, R.; Jin, Y.; Zhang, R. Zeolite Structure Effects on Cu Active Center, SCR Performance and Stability of Cu-Zeolite Catalysts. *Catal. Today* **2019**, *327*, 295−307.

(39) Kurbanova, A.; Zákutná, D.; Gołąbek, K.; Mazur, M.; Přech, J. Preparation of Fe@MFI and CuFe@MFI Composite Hydrogenation Catalysts by Reductive Demetallation of Fe-Zeolites. *Catal. Today* **2022**, *390−391*, 306−315.

(40) Li, S.; Tuel, A.; Laprune, D.; Meunier, F.; Farrusseng, D. Transition-Metal Nanoparticles in Hollow Zeolite Single Crystals as Bifunctional and Size-Selective Hydrogenation Catalysts. *Chem. Mater.* **2015**, *27*, 276−282.

(41) Hoang, D. L.; Dang, T. T. H.; Engeldinger, J.; Schneider, M.; Radnik, J.; Richter, M.; Martin, A. TPR Investigations on the Reducibility of Cu Supported on Al2O3, Zeolite Y and SAPO-5. *J. Solid State Chem.* **2011**, *184*, 1915−1923.

(42) Aylor, A. W.; Larsen, S. C.; Reimer, J. A.; Bell, A. T. An Infrared Study of No Decomposition over Cu-Zsm-5. *J. Catal.* **1995**, *157*, 592−602.

(43) Dědeček, J.; Wichterlová, B. Siting and Redox Behavior of Cu Ions in CuH-ZSM-5 Zeolites. Cu+ Photoluminescence Study. *J. Phys. Chem.* **1994**, *98*, 5721−5727.

(44) Huang, Y. Y. Selective Adsorption of Carbon Monoxide and Complex Formation of Cuprous-Ammines in Cu(I)Y Zeolites. *J. Catal.* **1973**, *30*, 187−194.

(45) Borovkov, V. Y.; Jiang, M.; Fu, Y. Investigation of Copper Carbonyl Species Formed upon CO Adsorption on Copper-Exchanged

Zeolites by Diffuse Reflectance FTIR. *J. Phys. Chem. B* **1999**, *103*, 5010−5019.

(46) Negri, C.; Borfecchia, E.; Martini, A.; Deplano, G.; Lomachenko, K. A.; Janssens, T. V. W.; Berlier, G.; Bordiga, S. In Situ X-Ray Absorption Study of Cu Species in Cu-CHA Catalysts for NH3-SCR during Temperature-Programmed Reduction in NO/NH3. *Res. Chem. Intermed.* **2021**, *47*, 357−375.

(47) Borfecchia, E.; Pappas, D. K.; Dyballa, M.; Lomachenko, K. A.; Negri, C.; Signorile, M.; Berlier, G. Evolution of Active Sites during Selective Oxidation of Methane to Methanol over Cu-CHA and Cu-MOR Zeolites as Monitored by Operando XAS. *Catal. Today* **2019**, *333*, 17−27.

(48) Paolucci, C.; Parekh, A. A.; Khurana, I.; Di Iorio, J. R.; Li, H.; Caballero, J. D. A.; Shih, A. J.; Anggara, T.; Delgass, W. N.; Miller, J. T.; et al. Catalysis in a Cage: Condition-Dependent Speciation and Dynamics of Exchanged Cu Cations in Ssz-13 Zeolites. *J. Am. Chem. Soc.* **2016**, *138*, 6028−6048.

(49) Williamson, W. B.; Flentge, D. R.; Lunsford, J. H. Ammonia Oxidation over Cu(II)NaY Zeolites. *J. Catal.* **1975**, *37*, 258−266.

(50) Deplano, G.; Martini, A.; Signorile, M.; Borfecchia, E.; Crocellà, V.; Svelle, S.; Bordiga, S. Copper Pairing in the Mordenite Framework as a Function of the CuI/CuII Speciation. *Angew. Chem., Int. Ed.* **2021**, *60*, 25891−25896.

(51) Henderson, G. S.; de Groot, F. M. F.; Moulton, B. J. A. X-Ray Absorption near-Edge Structure (XANES) Spectroscopy. *Rev. Mineral. Geochem.* **2014**, *78*, 75−138.

(52) Jones, R. G. X-Ray Absorption: Principles, Applications, Techniques of EXAFS, SEXAFS, and XANES. *Endeavour* **1988**, *12*, No. 195.

(53) Calvin, S. *XAFS for Everyone*; CRC Press, 2013.

(54) *X-Ray Absorption and X-Ray Emission Spectroscopy: Theory and Applications*; van Bokhoven, J. A., Lamberti, C., Eds.; John Wiley & Sons, Inc: Chichester, U.K., 2016.

(55) Marberger, A.; Petrov, A. W.; Steiger, P.; Elsener, M.; Kröcher, O.; Nachtegaal, M.; Ferri, D. Time-Resolved Copper Speciation during Selective Catalytic Reduction of NO on Cu-SSZ-13. *Nat. Catal.* **2018**, *1*, 221−227.

(56) Liu, C.; Kubota, H.; Amada, T.; Kon, K.; Toyao, T.; Maeno, Z.; Ueda, K.; Ohyama, J.; Satsuma, A.; Tanigawa, T.; et al. In Situ Spectroscopic Studies on the Redox Cycle of NH3−SCR over Cu−CHA Zeolites. *ChemCatChem* **2020**, *12*, 3050−3059.

(57) Bregante, D. T.; Wilcox, L. N.; Liu, C.; Paolucci, C.; Gounder, R.; Flaherty, D. W. Dioxygen Activation Kinetics over Distinct Cu Site Types in Cu-Chabazite Zeolites. *ACS Catal.* **2021**, *11*, 11873−11884.

(58) Rehr, J. J.; Ankudinov, A. L. Progress in the Theory and Interpretation of XANES. *Coord. Chem. Rev.* **2005**, *249*, 131−140.

(59) Guda, A. A.; Guda, S. A.; Lomachenko, K. A.; Soldatov, M. A.; Pankin, I. A.; Soldatov, A. V.; Braglia, L.; Bugaev, A. L.; Martini, A.; Signorile, M.; et al. Quantitative Structural Determination of Active Sites from in Situ and Operando XANES Spectra: From Standard Ab Initio Simulations to Chemometric and Machine Learning Approaches. *Catal. Today* **2019**, *336*, 3−21.

(60) Lamberti, C.; van Bokhoven, J. A.X-Ray Absorption and Emission Spectroscopy for Catalysis. In *X-Ray Absorption and X-Ray Emission Spectroscopy*; Wiley, 2015; Vol. 2, pp 351−383.

(61) Ravel, B.; Newville, M. ATHENA, ARTEMIS, HEPHAESTUS: Data Analysis for X-Ray Absorption Spectroscopy Using IFEFFIT. *J. Synchrotron Radiat.* **2005**, *12*, 537−541.

(62) Kuzmin, A.EDA: EXAFS Data-Analysis Software Package. In *International Tables for Crystallography*; Wiley, 2021.

(63) Meneghini, C.; Bardelli, F.; Mobilio, S. ESTRA-FitEXA: A Software Package for EXAFS Data Analysis. *Nucl. Instrum. Methods Phys. Res., Sect. B* **2012**, *285*, 153−157.

(64) Chupas, P. J.; Chapman, K. W.; Kurtz, C.; Hanson, J. C.; Lee, P. L.; Grey, C. P. A Versatile Sample-Environment Cell for Non-Ambient X-Ray Scattering Experiments. *J. Appl. Crystallogr.* **2008**, *41*, 822−824.

(65) Clark, A. H.; Imbao, J.; Frahm, R.; Nachtegaal, M. ProQEXAFS: A Highly Optimized Parallelized Rapid Processing Software for QEXAFS Data. *J. Synchrotron Radiat.* **2020**, *27*, 551−557.

(66) Zabinsky, S. I.; Rehr, J. J.; Ankudinov, A.; Albers, R. C.; Eller, M. J. Multiple-Scattering Calculations of x-Ray-Absorption Spectra. *Phys. Rev. B* **1995**, *52*, No. 2995.

(67) Wolfram Research, I. Mathematica. Wolfram Research, Inc.: Champaign, Illinois 2021.

(68) Pankin, I. A.; Martini, A.; Lomachenko, K. A.; Soldatov, A. V.; Bordiga, S.; Borfecchia, E. Identifying Cu-Oxo Species in Cu-Zeolites by XAS: A Theoretical Survey by DFT-Assisted XANES Simulation and EXAFS Wavelet Transform. *Catal. Today* **2020**, *345*, 125−135.

(69) Booth, C. H.; Hu, Y. J. Confirmation of Standard Error Analysis Techniques Applied to EXAFS Using Simulations. *J. Phys.: Conf. Ser.* **2009**, *190*, No. 012028.

(70) i Xamena, F. X. L.; Fisicaro, P.; Berlier, G.; Zecchina, A.; Palomino, G. T.; Prestipino, C.; Bordiga, S.; Giamello, E.; Lamberti, C. Thermal Reduction of Cu2+-Mordenite and Re-Oxidation upon Interaction with H2O, O2, and NO. *J. Phys. Chem. B* **2003**, *107*, 7036−7044.

(71) Lamberti, C.; Bordiga, S.; Salvalaggio, M.; Spoto, G.; Zecchina, A.; Geobaldo, F.; Vlaic, G.; Bellatreccia, M. XAFS, IR, and UV-Vis Study of the CuI Environment in CuI-ZSM-5. *J. Phys. Chem. B* **1997**, *101*, 344−360.

(72) Lamberti, C.; Bordiga, S.; Zecchina, A.; Salvalaggio, M.; Geobaldo, F.; Areán, C. O. XANES, EXAFS and FTIR Characterization of Copper-Exchanged Mordenite. *J. Chem. Soc., Faraday Trans.* **1998**, *94*, 1519−1525.

(73) Palomino, G. T.; Fisicaro, P.; Bordiga, S.; Zecchina, A.; Giamello, E.; Lamberti, C. Oxidation States of Copper Ions in ZSM-5 Zeolites. A Multitechnique Investigation. *J. Phys. Chem. B* **2000**, *104*, 4064−4073.

(74) Kim, J. Y.; Rodriguez, J. A.; Hanson, J. C.; Frenkel, A. I.; Lee, P. L. Reduction of CuO and Cu2O with H2: H Embedding and Kinetic Effects in the Formation of Suboxides. *J. Am. Chem. Soc.* **2003**, *125*, 10684−10692.

(75) Sun, X.; Sun, F.; Sun, Z.; Chen, J.; Du, X.; Wang, J.; Jiang, Z.; Huang, Y. Disorder Effects on EXAFS Modeling for Catalysts Working at Elevated Temperatures. *Radiat. Phys. Chem.* **2017**, *137*, 93−98.

(76) Artsiusheuski, M. A.; Verel, R.; van Bokhoven, J. A.; Sushkevich, V. L. Methane Transformation over Copper-Exchanged Zeolites: From Partial Oxidation to C-C Coupling and Formation of Hydrocarbons. *ACS Catal.* **2021**, *11*, 12543−12556.

(77) Deplano, G.; Signorile, M.; Crocellà, V.; Porcaro, N. G.; Atzori, C.; Solemsli, B. G.; Svelle, S.; Bordiga, S. Titration of Cu(I) Sites in Cu-ZSM-5 by Volumetric CO Adsorption. *ACS Appl. Mater. Interfaces* **2022**, *14*, 21059−21068.

(78) Alayon, E. M. C.; Nachtegaal, M.; Bodi, A.; Ranocchiari, M.; Van Bokhoven, J. A. Bis(μ-Oxo) versus Mono(μ-Oxo)Dicopper Cores in a Zeolite for Converting Methane to Methanol: An in Situ XAS and DFT Investigation. *Phys. Chem. Chem. Phys.* **2015**, *17*, 7681−7693.

(79) Castagnola, N. B.; Kropf, A. J.; Marshall, C. L. Studies of Cu-ZSM-5 by X-Ray Absorption Spectroscopy and Its Application for the Oxidation of Benzene to Phenol by Air. *Appl. Catal., A* **2005**, *290*, 110−122.

(80) Vennestrøm, P. N. R.; Janssens, T. V. W.; Kustov, A.; Grill, M.; Puig-Molina, A.; Lundegaard, L. F.; Tiruvalam, R. R.; Concepción, P.; Corma, A. Influence of Lattice Stability on Hydrothermal Deactivation of Cu-ZSM-5 and Cu-IM-5 Zeolites for Selective Catalytic Reduction of NOx by NH 3. *J. Catal.* **2014**, *309*, 477−490.

(81) Snyder, B. E. R.; Vanelderen, P.; Schoonheydt, R. A.; Sels, B. F.; Solomon, E. I. Second-Sphere Effects on Methane Hydroxylation in Cu-Zeolites. *J. Am. Chem. Soc.* **2018**, *140*, 9236−9243.

(82) Mahyuddin, M. H.; Staykov, A.; Shiota, Y.; Miyanishi, M.; Yoshizawa, K. Roles of Zeolite Confinement and Cu-O-Cu Angle on the Direct Conversion of Methane to Methanol by [Cu2(μ-O)]2+-Exchanged AEI, CHA, AFX, and MFI Zeolites. *ACS Catal.* **2017**, *7*, 3741−3751.

(83) Lamberti, C.; Spoto, G.; Scarano, D.; Pazé, C.; Salvalaggio, M.; Bordiga, S.; Zecchina, A.; Palomino, G. T.; D'Acapito, F. CuI-Y and CuII-Y Zeolites: A XANES, EXAFS and Visible-NIR Study. *Chem. Phys. Lett.* **1997**, *269*, 500−508.

(84) Palomino, G. T.; Bordiga, S.; Zecchina, A.; Marra, G. L.; Lamberti, C. XRD, XAS, and IR Characterization of Copper-Exchanged Y Zeolite. *J. Phys. Chem. B* **2000**, *104*, 8641−8651.

📖 Recommended by ACS

Structure of Selective and Nonselective Dicopper (II) Sites in CuMFI for Methane Oxidation to Methanol

Mikalai A. Artsiusheuski, Vitaly L. Sushkevich, *et al.*

DECEMBER 06, 2022
ACS CATALYSIS   READ 🗗

Investigation of the Active-Site Structure of Cu-CHA Catalysts for the Direct Oxidation of Methane to Methanol Using In Situ UV–Vis Spectroscopy

Yuka Tsuchimura, Junya Ohyama, *et al.*

JUNE 13, 2023
ENERGY & FUELS   READ 🗗

Tuning Copper Active Site Composition in Cu-MOR through Co-Cation Modification for Methane Activation

Dieter Plessers, Bert F. Sels, *et al.*

JANUARY 18, 2023
ACS CATALYSIS   READ 🗗

Isomorphously Substituted [Fe,Al]ZSM-5 Catalysts for Methane Dehydroaromatization

Yujie Liu, Nikolay Kosinov, *et al.*

JUNE 02, 2023
ACS CATALYSIS   READ 🗗

Get More Suggestions >